International Journal of Heat and Mass Transfer 54 (2011) 413–423

Contents lists available at ScienceDirect

International Journal of Heat and Mass Transfer

journal homepage: www.elsevier.com/locate/ijhmt

Enhanced heat exchanger design for hydrogen storage using high-pressure metal hydride: Part 1. Design methodology and computational results

Milan Visaria, Issam Mudawar *, Timothée Pourpoint

Hydrogen Systems Laboratory, Purdue University, West Lafayette, IN 47907, United States

ARTICLE INFO

Article history:
Received 24 February 2010
Received in revised form 18 August 2010
Accepted 18 August 2010
Available online 11 October 2010

Keywords:
Solid-state hydrogen storage
Heat exchanger
High-pressure metal hydride
$Ti_{1.1}CrMn$

ABSTRACT

This study explores the use of a high-pressure metal hydride (HPMH), $Ti_{1.1}CrMn$, to store hydrogen at high pressures (up to 310 bar) and temperatures below 60 °C, conditions that are suitable for automobile fuel cells. However, the exothermic reaction of hydrogen with this material releases large amounts of heat, and the reaction rate depends on the metal hydride temperature, decreasing significantly if the heat is not removed quickly. Therefore, a powerful heat exchanger constitutes the most crucial component of a HPMH hydrogen storage system. For automobiles, this heat exchanger must enable fueling 5 kg of hydrogen in less than 5 min. This is a formidable challenge considering the enormous amount of heat that must be released and the stringent limits on the heat exchanger's weight and volume, let alone a host of manufacturing requirements. Unlike conventional heat exchangers that are designed to exchange heat between two fluids, this heat exchanger is quite unique in that it must dissipate heat between a reacting powder and a coolant. In this first of a two-part study, a systematic heat exchanger design methodology is presented, starting with a 1-D criterion and progressing through a series of engineering decisions supported by computations of fill time. A final design is arrived at that meets the 5-min fill time requirement corresponding to minimum heat exchanger mass, supported by a 2-D computational model of the heat exchanger's thermal and kinetic response.

1. Introduction

With the increasing need for clean and sustainable energy options, interest in alternate fuels like hydrogen has never been higher. Hydrogen is both abundant in nature and has high gravimetric energy content. However, due to its low density, it poses major challenges in both storage and transport. Hydrogen can be stored as a very high-pressure gas or very low temperature liquid. Alternately, it can be stored in solid form by undergoing a chemical reaction into chemical hydrides, metal hydrides, or cryo-adsorbents [1–4]. Each of these storage techniques has its pros and cons, and the choice of a particular technique is dictated by the application. For automobiles, the system must be as compact and lightweight as possible. Another important practical requirement is that the time required to refuel a vehicle must be short. The Department of Energy (DOE) targets for onboard hydrogen storage is to charge 5 kg of hydrogen at the fueling station in less than 5 min by the year 2010 [5]; this amount of hydrogen covers a travel distance of 300 miles before needing to be refueled. In solid-state hydrogen storage, it is additionally important that the hydrogen be quickly and repeatedly released in response to the demands of the fuel cell or internal combustion engine. Presently, high-pressure metal hydrides (HPMHs) constitute one of the prime candidates for automotive hydrogen storage systems.

HPMHs that are suitable for hydrogen storage have the highest volumetric capacities compared to most other storage techniques [4]. With these materials, both the hydriding process (producing metal hydride by reaction of hydrogen gas with metal alloy) and dehydriding process (releasing the hydrogen from the metal hydride) are reversible and achievable at temperatures and pressures that are suitable for fuel cell use [2–4,6]. Although HPMHs have advantages over other storage techniques, they also pose several challenges. First, their low gravimetric capacity increases storage system weight [4,6]. Second, HPMHs must be handled and stored with extreme care. This is because for HPMHs to absorb hydrogen, they must first be pre-processed – activated – by breaking them into very fine particles. Among HPMHs, Ti–Cr–Mn-based metal hydrides are the most widely studied because of their cold-starting capability. Activating these hydrides requires breaking them to particles below 10 μm. However, once activated, they become pyrophoric and react readily in presence of air or moisture. Therefore, they must be stored and handled with extreme care, and sealed off from air or water before being packed into the storage system. Thirdly, and most importantly, the hydriding process is highly exothermic, with a temperature-dependent reaction rate that decreases significantly at high temperatures. In fact, the most crucial component of a HPMH storage system is a heat exchanger

* Corresponding author. Tel.: +1 765 494 5705; fax: +1 765 494 0539.
E-mail address: mudawar@ecn.purdue.edu (I. Mudawar).

0017-9310/$ - see front matter © 2010 Elsevier Ltd. All rights reserved.
doi:10.1016/j.ijheatmasstransfer.2010.09.029

Nomenclature

C_a	hydriding constant or activation rate (s^{-1})
c_p	specific heat (J/kg K)
E_a	activation energy (J/mol-H_2)
F	fraction of completion of reaction
ΔH_r	enthalpy of reaction (J/mol-H_2)
h	convective heat transfer coefficient (W/m^2 K)
k	thermal conductivity (W/m K)
L	metal hydride thickness (mm)
MW	molecular weight
P	pressure (N/m^2)
P_{eq}	equilibrium pressure (N/m^2)
P_o	ambient pressure (N/m^2)
$\dot{q}'''$	volumetric heat generation rate (W/m^3)
R	universal gas constant (8.314 J/mol K)
R_{tc}	contact resistance (mm^2 K/W)
ΔS	entropy of reaction (J/mol-H_2 K)
t	time (s)
T	temperature (K)
wt%	hydrogen to metal hydride mass ratio when completely hydrided
x	coordinate (mm)
y	coordinate (mm)

Greek symbols

μ	viscosity
ρ	density
φ	porosity

Subscripts

Al	Aluminum
eq	equilibrium
f	coolant
H_2	Hydrogen
MH	metal hydride
tot	total length used in 1-D model

that must remove the large amounts of heat released during the hydriding process.

Hydriding is a pressure and temperature dependent process associated with high heat of reaction. The $Ti_{1.1}CrMn$ used in the present study has a measured hydriding heat of reaction of about 14 kJ/mol-H_2 [4] and dehydriding heat of reaction around 22 kJ/mol-H_2 [7]. If at any time during the hydriding process the hydride temperature exceeds the temperature corresponding to equilibrium pressure, the reaction will stop and cannot proceed further until the temperature is brought once again below the equilibrium temperature. In addition, the rate of hydriding depends on the temperature of the hydride, the lower the hydride temperature the faster the reaction. Thus, the key to achieving fast refueling rates is to (1) quickly remove the heat released during hydriding and (2) maintain low metal hydride temperatures. Since the metal hydride itself has low gravimetric capacity, it is important that the heat exchanger and its components possess both high gravimetric efficiency and high volumetric efficiency (to maximize the volume available for the hydride). The DOE target for the gravimetric density of automobile storage systems is 4.5 wt% by the year 2010 [5]. To achieve this target, it is important to develop new and improved materials along with highly optimized heat exchanger and storage system designs.

For decades, heat exchangers have been extensively used in many diverse industrial applications. The most widely used heat exchangers are those intended to exchange heat between two fluids across a solid surface. These heat exchangers, like shell-and-tube, cross-flow, plate-type, etc., have been studied extensively for many decades. However, not much attention has been given to heat exchangers involving heat flow between a reacting powder and fluid across a solid surface. Design of this type of heat exchangers is becoming increasingly important with recent advances in nano-materials and powder metallurgy, let alone solid hydrogen storage.

A few recent heat exchanger studies related to metal hydride hydrogen storage have been focused on low-pressure complex metal hydrides [8–12], yet fewer studies address HPMH heat exchangers [4,6]. In this paper, which is the first of a two-part study, the detailed process of designing a reacting powder-to-fluid heat exchanger for storing hydrogen using HPMHs is discussed. Since HPMHs ignite spontaneously in the presence of air or moisture, their safe and reliable design is of utmost important. These heat exchangers must also be designed to operate at high pressure (up to 500 bar) and ensure leak-proof operation. A practical objective of the heat exchanger is to achieve a hydrogen fill time under 5 min using $Ti_{1.1}CrMn$ powder as storage material. In this part of this study, the detailed design methodology is discussed along with the computational model and computational results. The second part [13] will discuss the experimental methods used during the validation tests, present the experimental results, and compare them with computational results.

2. Heat exchanger design

2.1. 1-D and 2-D models

The key tool in initiating the design of the heat exchanger is a 1-D model that is used to calculate the "maximum thickness of metal hydride layer," which is the largest distance of hydride powder from a liquid-cooled aluminum surface such that the heat can be removed at a rapid rate that yields the desired reaction rate and a fill time of less than 5 min. Details of this 1-D model can be found in a recent study by the present authors [4]. Due to thermal symmetry, a layer of hydride contained between two aluminum surfaces can be assumed adiabatic along the centerline as shown in Fig. 1. The model accounts for contact resistance between the hydride powder and the aluminum surface. A convective boundary characterized by a coolant temperature and a convective heat transfer coefficient is assumed on the other side of the aluminum wall. As discussed in [4], the effects of hydride distance on hydride temperature, heat generation rate, and hydrogen fill time were ascertained by numerically solving the 1-D model using the properties and operating conditions listed in Table 1. Based on these results, the maximum thickness for $Ti_{1.1}CrMn$ was estimated at about 10 mm.

Fig. 2(a) illustrates the relevance of the 1-D maximum thickness to 2-D (plate-type) heat exchanger design. Since one boundary of the hydride is assumed adiabatic in the 1-D model, the critical thickness is actually half the distance between two cooling surfaces. Thus, a maximum thickness of 10 mm corresponds to a 20 mm distance between the cooling surfaces.

The high pressures required for HPMH storage systems preclude the use of the 2-D layout depicted in Fig. 2(a) or plate-type heat exchanger designs. Instead, only a cylindrical outer shape is permissible for this application since the heat exchanger must be inserted inside a cylindrical high-pressure vessel. Overall, the heat

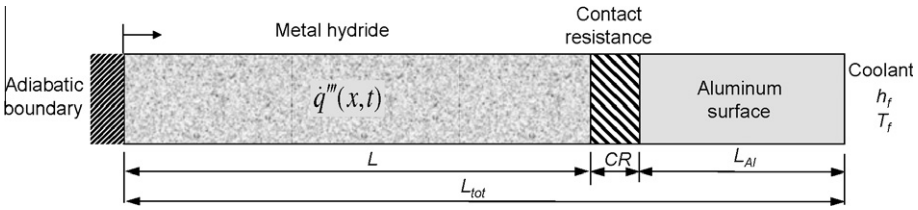

Fig. 1. 1-D model setup for heat exchanger design.

Table 1
Metal hydride properties and coolant conditions used in model.

Kinetic	
Activation energy	Ea = 20.7 kJ/mol of H_2
Enthalpy of formation	ΔHr = −14,390 J/mol of H_2
Entropy of formation	ΔS = −91.3 J/mol of H_2
Activation rate	Ca = 150 s^{-1}
H_2 storage capacity	1.5 wt%
Thermal	
Packing density	ρ_{MH} = 2500 kg/m^3
Effective thermal conductivity	k_{MH} = 1 W/m K
Specific heat	$c_{p,MH}$ = 500 J/kg K
Contact resistance	R_{tc} = 2000 mm^2 K/W
Coolant	
Temperature	T_f = 0 °C
Convection coefficient	h_f = 2500 W/m^2 K

exchanger must adhere to four practical vehicle manufacturer design guidelines:

(1) Cylindrical external shape.
(2) Aluminum construction.
(3) Single coolant U-tube.
(4) Two-dimensional shape that lends itself to cost-effective fabrication techniques such as extrusion.

Ideally, a highly efficient "extruded" design is desired in which the hydride is housed in small "cells" that are cooled by a network of fins that effectively channel the heat to the coolant U-tube as illustrated in Fig. 2(b). Assuming very high fin efficiency for the time being, the usefulness of the 1-D maximum hydride thickness model lies in the sizing of the individual hydride cells. As indicated in Fig. 2(b) for two different cells, the center of the cell corresponds to the hydride point farthest from the aluminum surface and must therefore satisfy the maximum thickness criterion as a staring point in the heat exchanger design.

2.2. Design progression

Achieving the maximum hydride thickness criterion while attempting to minimize heat exchanger weight and volume are two opposing design trends. The first requires using aluminum fins throughout the metal hydride, which tends to increase heat

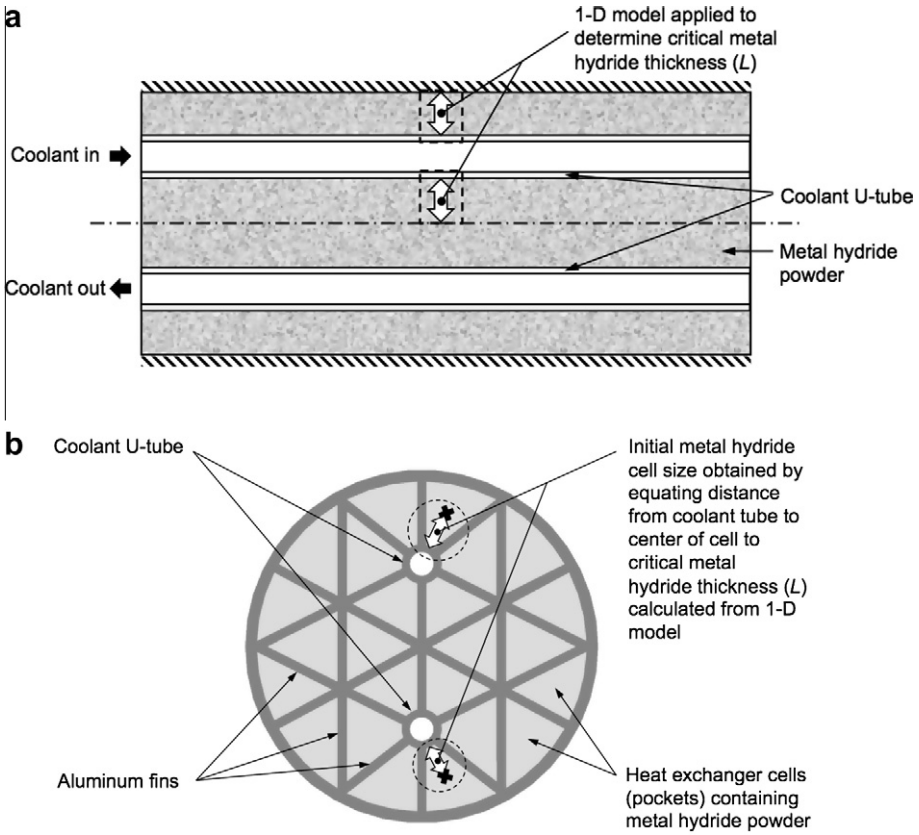

Fig. 2. Relevance of 1-D maximum hydride layer thickness model to design of (a) 2-D plate-type and (b) cylindrical metal hydride heat exchangers.

exchanger weight and volume. Hence, it is important that the fin structures be as thin and thermally efficient as possible. Following is a discussion of an iterative design progression that was used in pursuit of this goal.

Fig. 3(a)–(d) show the steps taken in the heat exchanger design progression, and the volume occupied by the heat exchanger as a fraction of the pressure vessel (PV) volume before reaching the final design. The procedure involves designing the heat exchanger and calculating the fill time using a two-dimensional Fluent model (details of this model will be discussed later). If the calculated fill time is less than 5 min, the design is optimized by reducing fin mass. However, if the fill time of 5 min is not achieved, either the fin mass is increased or the fin distribution altered. This process continues until an optimum heat exchanger design is obtained which achieves a fill time below 5 min.

Fig. 3(a) shows an initial heat exchanger design using 5-mm thick fins, which occupies 39% of the pressure vessel volume. For this design, the Fluent model predicts a fill time of 4.5 min, which implies the heat exchanger performance can be improved by rearranging fins and/or reducing fin thickness. Fig. 3(b) shows a subsequent design in which the fin thickness is reduced to 2 mm and some fins are removed or repositioned. While the heat exchanger now occupies only 24.9% of the pressure vessel volume, the fill time exceeds 5 min. Upon examining transient temperature results, several locations were detected where insufficient cooling caused the hydriding reaction to slow and stop altogether, resulting in longer overall fill times. Those 'hot spots' were eliminated by strategic placement of fins and, more importantly, by compartmentalizing the hydride powder into cells surrounded by fins on all sides to provide a more uniform heat transfer path from all directions. This modification can be observed in the transition between the designs in Fig. 3(b) and (c). Locations closer to the coolant tubes react faster due to higher heat transfer rates. As a result, cells closer to the coolant tubes are made larger compared to the cells farther from the coolant tubes. The heat exchanger design in Fig. 3(c) occupies 33.1% of pressure vessel volume using a fin thickness of 3 mm and achieves a fill time of 5 min.

Fin efficiency can be improved further by using radial fins originating directly from the coolant tube rather than using branching fins. Fig. 3(d) shows the final heat exchanger design in which all the fins originate from the coolant tube. With this design, which satisfies the 5 min fill time, the heat exchanger occupies only 29% of the pressure vessel volume, 25% smaller than the design in Fig. 3(a). This demonstrates the effectiveness of the design optimization methodology.

Overall, there is a narrow range for optimum fin thickness. Below this range, the fin cannot provide sufficient conduction path, and above this range, the size of the heat exchanger increases without a noticeable improvement in performance. These considerations lead to an optimum fin thickness between 2 and 3 mm. Also, because metal hydride powder can expand during hydriding and contract during dehydriding by as much as 30%, it can exert high stresses on the heat exchanger fins. The 2–3 mm thickness is deemed adequate to withstand these stresses.

2.3. Final design

The iterations and optimization that culminated in the design shown in Fig. 3(d) was modified to the one shown in Fig. 3(e) for experimental validation purposes. Both designs are identical except for six circumferential holes that were required for experimental assembly. The following section discusses details of the prototype heat exchanger that was used in the experimental validation tests.

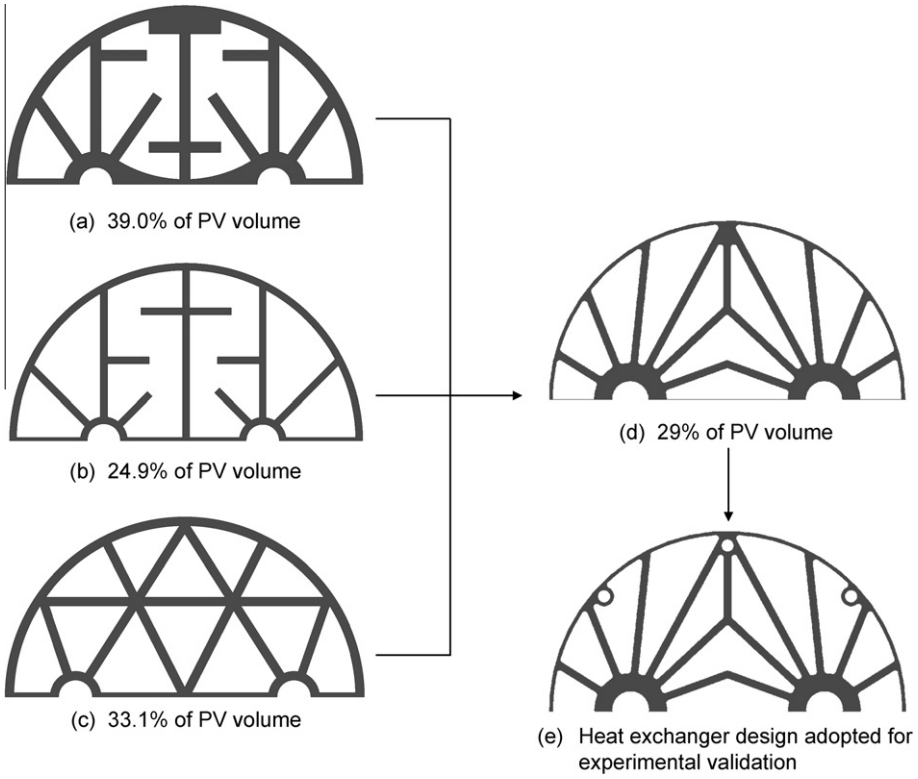

Fig. 3. Progression of heat exchanger designs.

3. Prototype heat exchanger construction and instrumentation

3.1. Heat exchanger plates

To assess the heat exchanger's performance and compare it to computational results, a 260.3-mm (10.25-in.) long prototype was fabricated. With a metal hydride density of 2500 kg/m^3, the heat exchanger could store 2.65 kg of metal hydride powder.

As discussed earlier, one of the practical design guidelines of the heat exchanger is a two-dimensional construction that lends itself to cost-effective fabrication techniques such as extrusion. Because of the need to instrument the metal hydride cells with thermocouples at several strategic locations, the solid extruded structure of the heat exchanger was replaced by a series of 6.35-mm (0.25 in.) thick aluminum 6061 plates – slices – having the identical cross-section and material as the extrusion. The plates were fabricated by CNC machining. Fig. 4 shows the cross-section of the heat exchanger plates. It has a network of fins radiating from the coolant tube, forming cells where the metal hydride powder is filled.

3.2. Tapered collet

Contact resistance between the heat exchanger plates and the coolant tube was minimized by using tapered collets around the coolant tubes. Fig. 5 shows the detailed construction of the collet. It is a hollow, cylindrical tube with an inner diameter slightly larger than the outer diameter of the coolant tube, and is tapered on the outside. Three 1-mm slots run most of the collet length save for two threaded ends, where support hexagonal nuts are connected. The collet has a bidirectional taper of 1.2°, such that its diameter increases from the two ends towards the center, where the diameter is largest. Having a bidirectional taper instead of a unidirectional one reduces the maximum diameter of the collet by half. The tapered portion of the collet is 254-mm (10-in.) long and each half holds 20 heat exchanger plates. The holes in the heat exchanger plates through which the coolant tube and collets pass are also tapered at the same angle to match the collet taper. The outer diameter of the collet taper is a few thousandths of an inch larger than the diameter of the heat exchanger plate holes to achieve interference fit and hence good contact between the two.

During assembly, the collets are first slid over each leg of the coolant U-tube, and the heat exchanger plates pushed axially inwards towards the center the collets. The longitudinal slots allow the collet to compress on the coolant tube as the hexagonal nuts on the end of the collet press the plates axially towards the center. This results in excellent mechanical and thermal contact between the heat exchanger plate and the collets and coolant tube.

3.3. Cover plates

The heat exchanger is fitted with two cover plates, which are attached as shown in Fig. 6. Aside from sealing the two ends of the heat exchanger, the cover plates contain hydrogen and coolant fittings as well as thermocouple feed-through. Made from 304 stainless steel, the cover plates contain five fittings each: two for the coolant U-tube, two for check valves, and one for a thermocouple feed-through. The check valves play the dual role of (1) preventing air from flowing into the containment vessel as the heat exchanger is being transported from the glove box to the pressure vessel, and (2) allowing hydrogen gas to enter the containment vessel during testing. A circular cavity within each cover plate provides space for a diffuser plate. This plate is a sintered disk made from 316 stainless steel with 30% porosity and 10-μm pore size. Its purpose is to distribute hydrogen gas uniformly to all the heat exchanger cells as it flows through the two check valves, as well as to serve as a filter for the metal hydride powder. Additional filtering is provided by sheets of filter paper placed between the cover plate and the adjacent heat exchanger plate.

3.4. Heat exchanger test assembly

Figs. 6 and 7 depict CAD renderings of the heat exchanger assembly without the containment vessel. Some heat exchanger plates are omitted in Fig. 7 to show internal details. Notice that in addition to the 40 aluminum heat exchanger plates, a Teflon

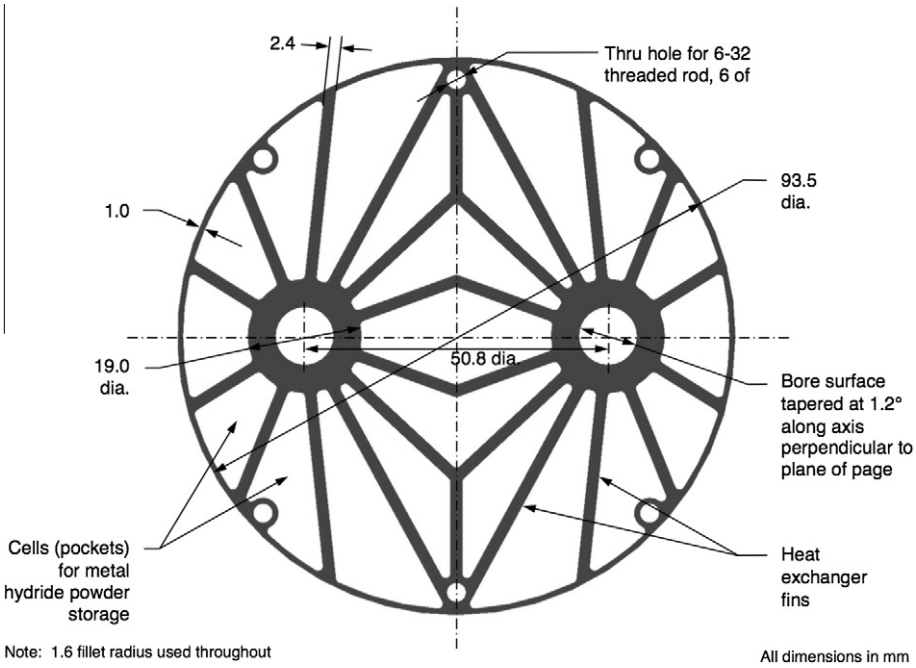

Fig. 4. Cross-sectional view of heat exchanger plate.

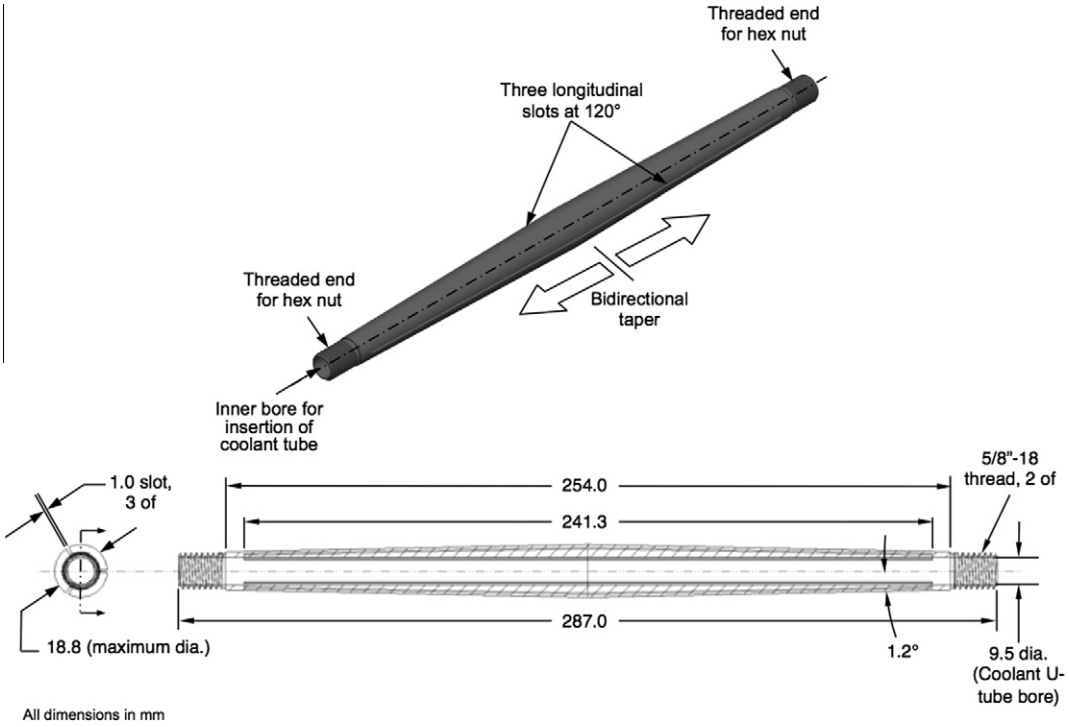

Fig. 5. Isometric view and detailed drawing of tapered collet.

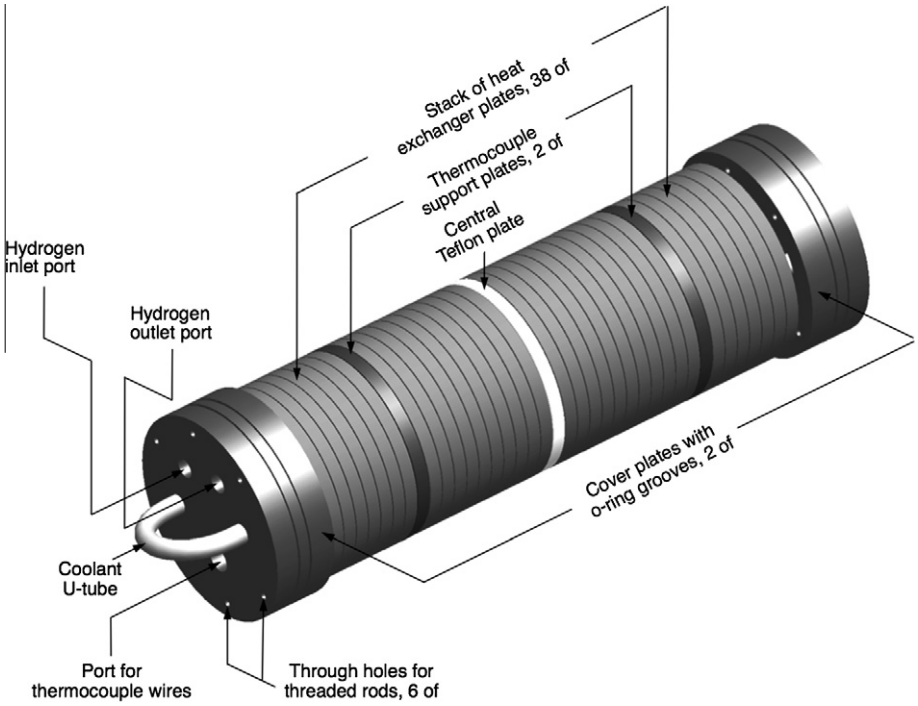

Fig. 6. 3-D rendering of heat exchanger assembly.

plate similar in design to the other plates is added in the center. The softer Teflon material allows for any axial mismatch in the taper of the collet and heat exchanger plate holes to be rectified. Two heat exchanger plates are modified with stainless steel posts to mount thermocouples at precise locations within the metal hydride powder. These plates are placed one quarter and three quarters along the length of the heat exchanger.

4. Computational model

4.1. Model description

Tests were performed that provided a fairly uniform fluid temperature along the coolant tube. Most operating conditions produced a total temperature drop between the inlet and outlet of

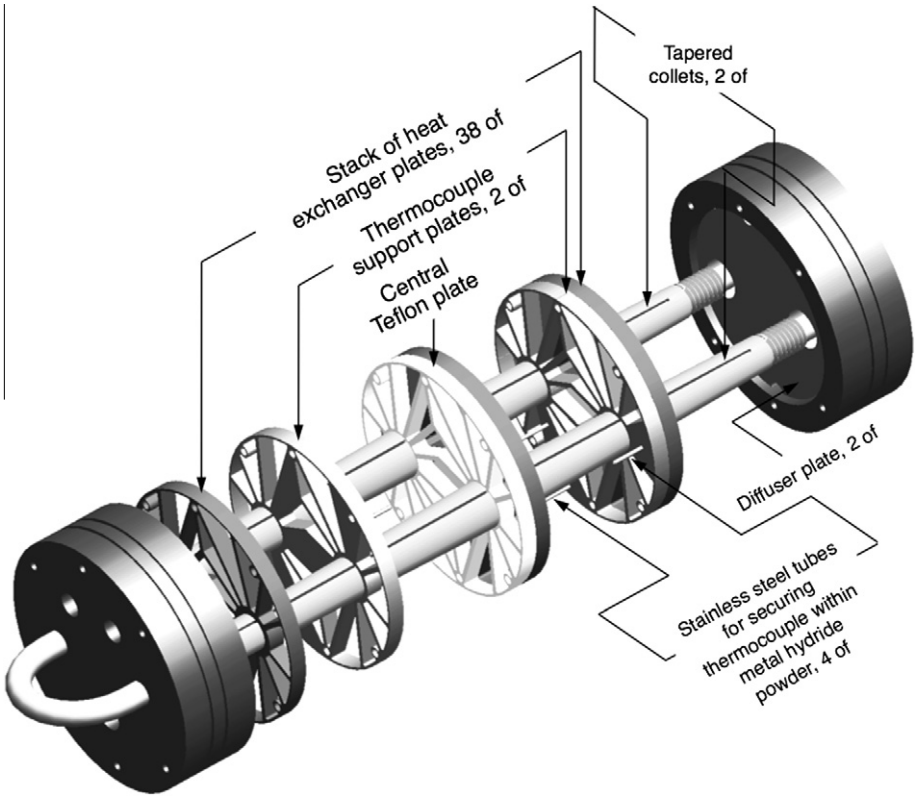

Fig. 7. Detailed 3-D rendering of heat exchanger assembly.

the coolant tube of less than 0.5 °C with a worst case of 1.5 °C. These operating conditions produced a fairly 2-D temperature distribution within the heat exchanger's cross-section, which also simplified the understanding and prediction of the metal hydride kinetics.

The domain of the 2-D Fluent model employed in this study is a cross-section of the heat exchanger shown as in Fig. 3(e). Since the upper and lower halves are thermally symmetrical, only one half is modeled to reduce computing time. The heat exchanger is made of aluminum 6061-T6 and the cells are filled with $Ti_{1.1}CrMn$ powder. The network of fins dissipates the heat generated from the metal hydride powder during hydriding to the coolant flowing through the U-tube. Since the heat exchanger plates are enclosed in 316 stainless steel containment vessel and encased in a low thermal conductivity nylon sleeve before the entire assembly is finally inserted in the high pressure vessel for testing, the model assumes an adiabatic outer boundary for the heat exchanger. Thus, in the model, all the heat generated during the hydriding is removed by the coolant.

Assuming the hydride has constant and isotropic properties, the temperature at any location within the hydride can be defined by two-dimensional transient heat conduction with internal heat generation. The heat diffusion equations for the aluminum and the hydride are given, respectively, by

$$k_{Al}\left(\frac{\partial^2 T}{\partial x^2}+\frac{\partial^2 T}{\partial y^2}\right)=\rho_{Al}c_{p,Al}\frac{\partial T}{\partial t} \tag{1}$$

and

$$k_{MH}\left(\frac{\partial^2 T}{\partial x^2}+\frac{\partial^2 T}{\partial y^2}\right)+\dot{q}'''=\rho_{MH}c_{p,MH}\frac{\partial T}{\partial t}, \tag{2}$$

where k_{Al}, ρ_{Al} and $c_{p,Al}$ are the thermal conductivity, density and specific heat of the aluminum, respectively, k_{MH}, ρ_{MH} and $c_{p,MH}$ are the effective thermal conductivity, density and specific heat of the metal hydride powder, respectively, and $\dot{q}'''$ is the rate of volumetric heat generation in the hydride. Eqs. (1) and (2) are solved in Fluent to obtain the temperature distribution across the domain. The heat generation in Eq. (2) is the sum of heat of reaction and heat of pressurization (accounts for less than 10% of the total heat generated).

$$\dot{q}'''=\frac{dF}{dt}\frac{(\mathrm{wt}\%)\rho_{MH}}{MW_{H_2}}\Delta H_r+\phi\frac{dP}{dt}, \tag{3}$$

where F, MW_{H_2}, ΔH_r, ϕ and P are the fraction of completion of reaction, molecular weight of hydrogen, enthalpy of reaction, porosity and pressure, respectively. As indicated in Eq. (3), the rate of heat generation depends on the rate of hydriding, the faster the reaction rate the higher the heat generation rate. The reaction rate is computed using an expression for hydrogen absorption in $LaNi_5$ derived by Mayer et al. [14] which assumes 1st order kinetics typically observed in metal hydrides.

$$\frac{dF}{dt}=C_a\exp\left(\frac{-E_a}{RT}\right)\ln\left(\frac{P}{P_{eq}}\right)(1-F), \tag{4}$$

where C_a, E_a, R and P_{eq} are the hydriding constant, activation energy, universal gas constant and equilibrium pressure, respectively. Eq. (4) helps explain the effects of pressure and hydride temperature on the rate of reaction and, hence, heat generation rate. The reaction cannot proceed until the pressure within the storage system exceeds the equilibrium pressure and stops once the pressure falls below equilibrium. Because P_{eq} increases with increasing T, the reaction rate is slower at higher hydride temperature and, to accelerate the reaction rate, it is necessary to lower the hydride temperature. This can be further explained by the metal hydride temperature and equilibrium pressure plots in Fig. 8. The metal hydride powder far from the cooling surface is at a relatively high temperature and, therefore, has higher equilibrium pressure. The

small difference between the pressure vessel pressure and the equilibrium pressure causes reaction rate to be slow for metal hydride in these locations; the reaction even stops when the two pressures are equal. However, for metal hydride powder close to the cooling surface, the difference between the two pressures is greater and, therefore, the reaction rate is faster. Eq. (4) also indicates that hydriding is a self-limiting reaction, that is, as the reaction progresses its rate slows down.

Equilibrium pressure is the minimum pressure at a given temperature at which hydriding can occur, and is given by the van't Hoff equation

$$P_{eq} = P_o \exp\left(\frac{\Delta H_r}{RT} - \frac{\Delta S}{R}\right), \quad (5)$$

where P_o and ΔS are the ambient pressure and entropy of reaction, respectively. The equilibrium pressure increases rapidly with increasing metal hydride temperature. It is therefore important to maintain high pressures along with low hydride temperatures to achieve fast fill rates.

The above Eqs. (1)–(5) are solved simultaneously in Fluent to determine the transient variation of metal hydride temperature, reaction progress, and volumetric heat generation rate.

4.2. Metal hydride properties

In order for $Ti_{1.1}CrMn$ to absorb hydrogen, it must first be activated by breaking it into very fine particles. Activation is achieved by subjecting metal hydride powder to repeated cycles of high-pressure cooling and low-pressure (vacuum) heating, which is described in detail in the second part of this study [13]. Fig.9 shows SEM images of the $Ti_{1.1}CrMn$ powder before and after the activation process. Notice how the activation process drastically reduces the average metal hydride particles size from 72 μm to less than 10 μm.

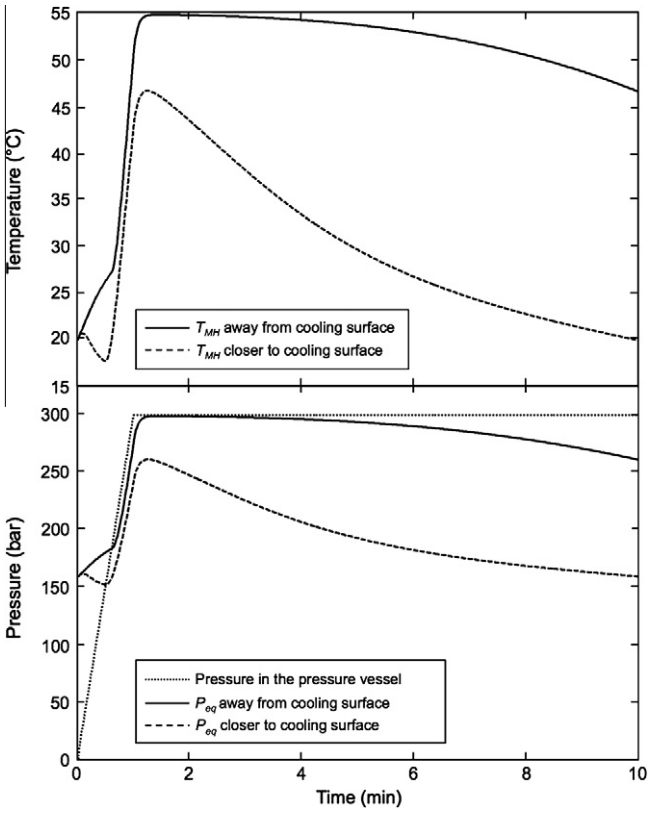

Fig. 8. Variation of equilibrium pressure with metal hydride temperature.

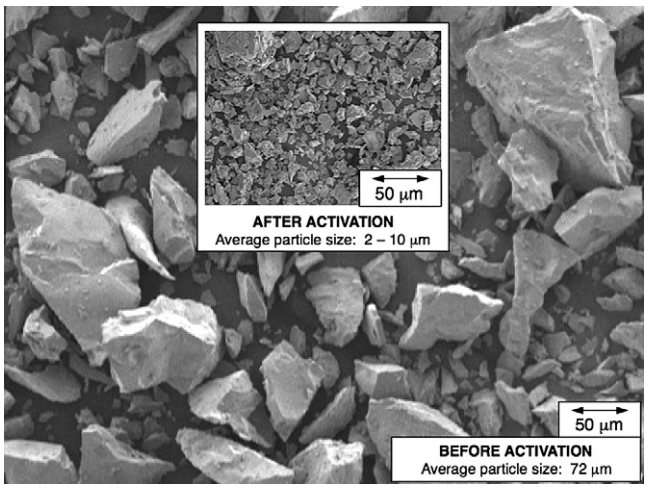

Fig. 9. SEM images of $Ti_{1.1}CrMn$ (a) before activation and (b) after activation.

The properties of $Ti_{1.1}CrMn$ were measured at the Purdue University Hydrogen Systems Laboratory (HSL) at pressures ranging from atmospheric to 253 bar. The kinetic and thermal properties of $Ti_{1.1}CrMn$ are listed in Table 1 and the thermal properties of aluminum 6061-T6 are given in Table 2. Experimental property measurements of HPMHs are extremely challenging because of the high pressures involved (~300 bar), their pyrophoric behavior and sensitivity to impurities. Flueckiger et al. [15] used the transient plane source (TPS) technique to measure thermal properties of $Ti_{1.1}CrMn$. This technique employs a resistive element as both a heat source and a temperature sensor, which is sandwiched between two identical hydride powder samples. The temperature response and change in electrical resistance of the element in response to a heat pulse are correlated to the thermal properties of hydride powder [15–16]. Flueckiger et al. measured the thermal conductivity and calculated the specific heat of activated $Ti_{1.1}CrMn$ (with 70% porosity) at temperatures ranging from 14 to 18 °C and pressure up to 275 bar from thermal diffusivity measurements using the TPS technique. Before the onset of hydriding (170 bar at room temperature), k_{MH} increased from 0.3 to 0.7 W/m K with increasing pressure. While during the hydriding phase (above 170 bar), k_{MH} was constant at 0.7 W/m K. In general, k_{MH} depends on factors as particle size, packing density (porosity), and hydride temperature, which should increase k_{MH} under the operating conditions of the present study compared to those of Flueckiger et al. One reason for this increase is the higher packing density (60% porosity) used in this study compared to the measured samples. Another reason is the much higher metal hydride temperature during the hydriding reaction for the present study (about 50 °C) compared to 14–18 °C for the measured samples. It is also noteworthy that Suda et al. [17] measured an increase in k_{MH} for $TiMn_{1.5}$ from 0.5 to 1.2 W/m K as hydrogen pressure was increased from 0.5 to 40 bar. Therefore, a constant value of $k_{MH} = 1$ W/m K is used in the present study, which lies between the two measurement ranges.

Table 2
Properties of aluminum 6061-T6.

Density ρ_{Al} (kg/m^3)	Specific heat $c_{p,Al}$ (J/kg K)	Conductivity k_{Al} (W/m K)
2719	871	202

Flueckiger et al. calculated $c_{p,MH}$ for $Ti_{1.1}CrMn$ samples in the range of 400 and 600 J/kg K up to 80% hydrided state. Above 80%, they calculated an abrupt jump in $c_{p,MH}$ to 1000 J/kg K. They attributed this jump to phonon transport at the hydrogen occupied interstitials of the metal hydride lattice. Since $c_{p,MH}$ was calculated between 400 and 600 J/kg K for major part of the hydriding reaction, in present model a constant value of $c_{p,MH}$ = 500 J/kg K is used.

Contact resistance is very difficult to measure or ascertain and its magnitude depends on particle size, packing density, physical properties of aluminum interface and pressure between the power and the aluminum surface. Recently, contact resistance measurements were performed at the Purdue Hydrogen Systems Laboratory using the TPS technique. Contact resistances between a Kapton-coated resistive element and a metal hydride powder bed ranged from R_{tc} = 400 to 1800 mm^2 K/W with 30% uncertainty. However, these measurements cannot replicate the continuous expansion and contraction of hydride powder during repeated cycling in actual tests, which is expected to increase contact resistance with the aluminum surfaces. Therefore, a constant value of R_{tc} = 2000 mm^2 K/W is used in the present study.

Some of the kinetic properties of $Ti_{1.1}CrMn$, like activation energy, E_a, were obtained from the literature while others, like enthalpy of reaction, ΔH_r, and entropy of reaction, ΔS, were measured at the Purdue University Hydrogen Systems Laboratory. From the pressure composition isotherm (PCT), the maximum hydrogen storage capacity of $Ti_{1.1}CrMn$ powder to be used for experimental work was measured at 1.5 wt% corresponding to 280 bar.

In the absence of detailed kinetic property measurements for HPMHs, the activation energy of $Ti_{1.1}CrMn$ is estimated from measurements by Suda et al. [18] for $LaNi_5$ of E_a = 20.7 kJ/mol-H_2.

For $LaNi_5$, Suda et al. also measured an activation rate of C_a = 54.7 s^{-1}. However, experiments performed at the Hydrogen Systems Laboratory suggest $Ti_{1.1}CrMn$ possesses better kinetics than $LaNi_5$, with a C_a value closer to 150 s^{-1}. Nonetheless, the authors of the present study have conducted a sensitivity analysis of different kinetic and thermal properties of $Ti_{1.1}CrMn$ and demonstrated that C_a has an unusually small influence on reaction rate [4]. By increasing C_a from 150 to 10,000 s^{-1}, they calculated a change of less than 1 min in reaction time.

Using Eq. (5) over the entire range of the reaction, and the variation of the metal hydride temperature with pressure obtained from previously performed experiments, the enthalpy of hydriding reaction of $\Delta H_r = -14.4$ kJ/mol-H_2 and entropy change of $\Delta S = -91.3$ kJ/mol-H_2 were measured.

The coolant used in the model is Dex-Cool®, which is commercially available automotive antifreeze whose properties are listed in Table 3. In the model, coolant is assumed to be flowing at a constant temperature of 0 °C. The chiller to be used in the experiments has a maximum coolant flow rate of 15 lpm, from which the convective heat transfer coefficient in the U-tube was calculated as 2500 W/m^2 K, the value used in the Fluent model. It is further assumed in the model that, initially the hydride is in a completely dehydrided state and at 20 °C. The pressurization profile assumed in the model is a linear ramp from atmospheric pressure to 300 bar in 60 s, and a constant pressure of 300 bar thereafter until the hydriding process is completed.

5. Computational results

The heat exchanger is designed with the objective of achieving a fill time of less than 5 min. Fill time refers to the time necessary for the entire metal hydride to complete 90% of the hydriding reaction on a volume-averaged basis. The computation model provides a tool to compare various heat exchanger designs and predict the fill time that can then be verified by experiment. The performance of the final heat exchanger design in Fig. 3(e) is analyzed herein. Variation of temperature, $T(x, y, t)$, reaction progress, $F(x, y, t)$, and heat generated, $\dot{q}'''(x, y, t)$ from the start of the pressurization until the end of hydriding reaction are discussed in this section. Fig. 10 shows color contour plots of these three parameters over time during the hydriding phase superimposed on a cross-section of the heat exchanger.

Notice that for the first 20 s, no reaction takes place. Initially, the metal hydride is at 20 °C and the corresponding equilibrium pressure is 160 bar. Hence, unless the pressure increases above 160 bar or the hydride temperature decreases such that the equilibrium pressure is below the pressure vessel pressure, the hydriding reaction will not start. Until then the only source of heating is pressurization, which results in a small hydride temperature raise at 20 s. At 40 s, when the pressure is 200 bar, heat is generated from the metal hydride due to the hydriding reaction. Up to 2 MW/m^3 of heat is generated in small cells and close to the aluminum fins while the heat generation rate is closer to 1 MW/m^3 in the interior of larger cells. Associated with this heat generation is an increase in the temperature of the metal hydride to 35 °C. At 60 s, the pressurization ramp is complete and peak heat generation rate reaches 3.5 MW/m^3. Notice how the metal hydride is now reacting faster around the coolant tubes and near the fins, where heat transfer rates are highest and the temperatures lowest. The temperatures in the middle of the cells are at 48 °C while, near the fins, they are about 40 °C. Also at 60 s, the metal hydride around the coolant tubes and near the fins has completed 30% of the reaction while, away from the fins, it has just begun hydriding. At 60 s, heat generation is highest during the hydriding process since after 60 s the pressure remains constant and no additional heating is generated due to pressurization. Furthermore, with no further increase in pressure after 60 s, the only way to increase the reaction rate and hence the heat generated rate is by lowering the hydride temperature. Therefore, once the pressurization ramp is completed, a drop in the reaction rate ensues. At 100 s, the metal hydride temperature is fairly uniform in all cells at 55 °C. The sections of fins close to the coolant tubes are at ~38 °C while the sections farthest from the coolant tube along the outer periphery are ~45 °C. Around the coolant tubes, heat generation rate is ~1.5 MW/m^3 and in the longer cells less than 0.5 MW/m^3; the metal hydride located up to 10 mm from the coolant tubes has completed 50% of the reaction.

At 300 bar, the equilibrium temperature of $Ti_{1.1}CrMn$ is 55 °C. Hence at 55 °C the hydride stops reacting. As the metal hydride powder cools below 55 °C, it starts hydriding again, thereby generating heat and increasing in temperature. For further hydriding to take place, the metal hydride needs to be cooled again to maintain the temperature below equilibrium. This process continues until the hydride completes the reaction. As time progresses from 100

Table 3
Properties of Dex-Cool®.

Temperature T (°C)	Density ρ_f (kg/m^3)	Specific heat $c_{p,f}$ (J/kg K)	Conductivity k_f (W/m K)	Viscosity μ_f (Pa s)
0	1068	3460	0.415	7.26×10^{-3}
20	1059	3570	0.428	3.39×10^{-3}

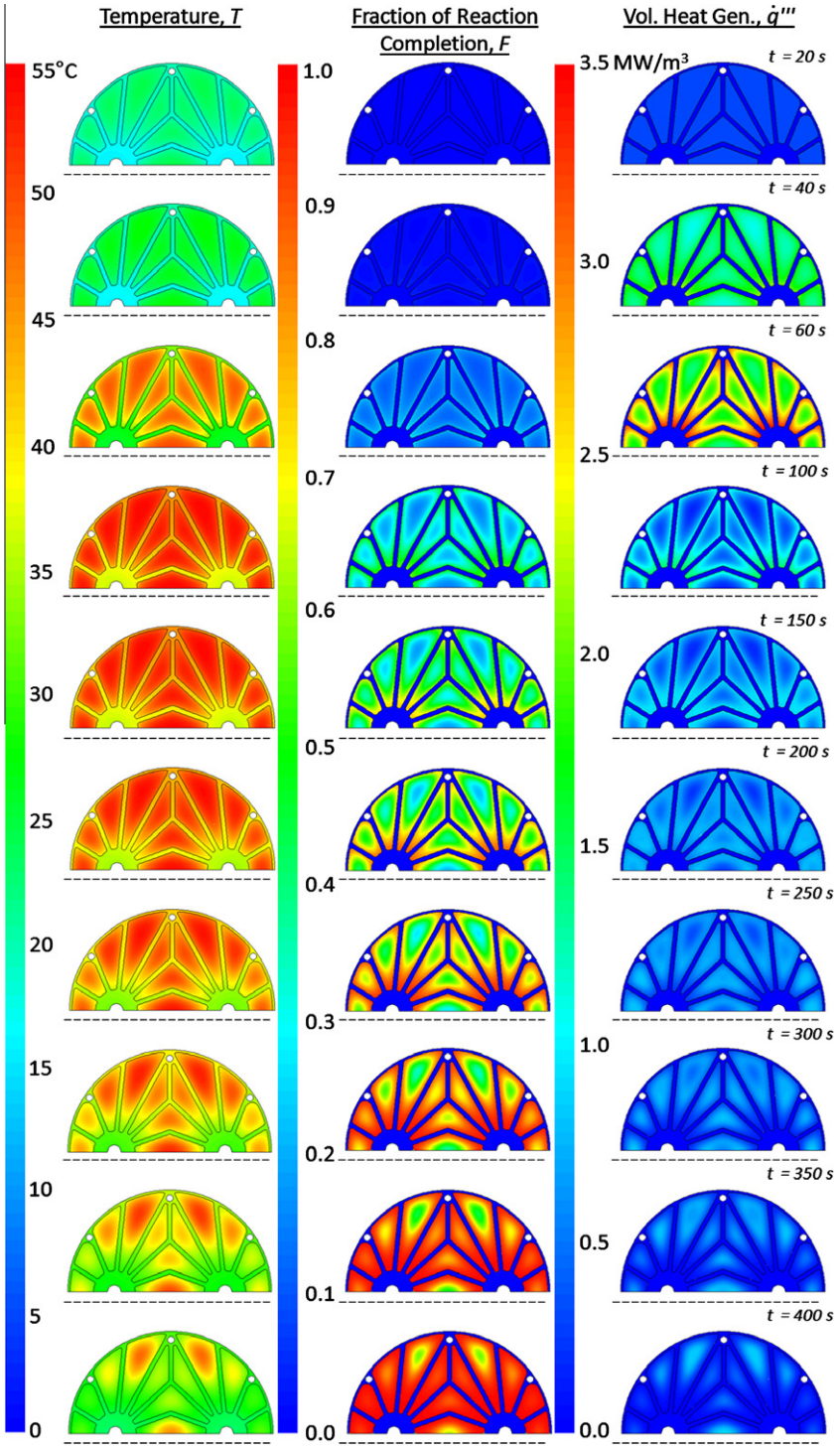

Fig. 10. Transient contours of temperature, fraction of reaction completion and volumetric heat generation rate during hydriding.

to 300 s, the coolant continues removing heat from the metal hydride while the hydriding reaction progresses further from the periphery of the cells to the interior. At 300 s, the heat generated ranges from 0.5 to 1 MW/m^3 due to the reduced reaction rate. This is primarily due to two reasons. The first is the still elevated hydride temperatures in the core of the larger cells. To achieve fast reaction rates, it is very important that the hydride temperature be significantly lower than the equilibrium temperature. Larger cell widths result in low heat transfer rates to the metal hydride deep within the cells causing slower reaction rates in these locations. This demonstrates the importance of the metal hydride thickness criterion in the design of the heat exchanger. The second reason for reduced reaction rate is the self-limiting nature of the reaction that causes a decrease in the rate of reaction as it progresses. At 300 s, excepting the core region of a few large cells where the hydride has completed 60% of reaction, the metal hydride is completely hydriding everywhere else. At the end of 300 s, the metal hydride has stored 90% hydrogen of its maximum

capacity. If the reaction is allowed to continue further by maintaining the pressure, the remaining hydride will eventually cool down to a uniform temperature, thus completing the hydriding process.

While the computational model provides that the heat exchanger design can achieve the desired fill time of 5 min, both the design and the model will require experimental validation. The second part of the study [13] will discuss the experimental methods used during the validation tests, present the experimental results, and compare the experimental and computational results.

6. Conclusions

This paper presented a methodology for the design of a heat exchanger for hydrogen storage using high-pressure metal hydrides (HPMHs). A simple, yet powerful 1-D criterion for maximum metal hydride thickness served as a guide for initiating the heat exchanger design. This is followed by an iterative design approach to meet specific design goals, guided by a 2-D computational model. Key conclusions from the study are as follows:

1. The heat exchanger is the most crucial component of a hydrogen storage system utilizing a HPMH. The primary function of the heat exchanger is to remove the large amounts of heat released from the hydriding reaction as the system is being filled with hydrogen at the station. The heat exchanger design must adhere to several design criteria including removing the heat in less than 5 min, compact and lightweight design, and cost and ease of manufacturability.
2. Using a single coolant U-tube and standard 101.6-mm (4-in.) pressure vessel for hydrogen storage, an iterative design culminated in an extruded aluminum construction with thin fins radiating from the coolant tube and forming cells inside which the HPMH powder is stored. The final design occupies 29% of the pressure vessel volume, leaving the remaining volume for the metal hydride powder. Further enhancement in the thermal performance of the heat exchanger is achieved with the aid of tapered collets that help eliminate contact resistance between the coolant tube and the heat exchanger parts.
3. A 2-D model provides a detailed understanding of the spatial and temporal response of the metal hydride's temperature, reaction rate and heat generation rate. The hydriding reaction proceeds only when its temperature is lower than the equilibrium temperature or the pressure is above the equilibrium pressure. Colder portions of the metal hydride close to the fin surface start hydriding earlier and finish hydriding before the warmer portions away from the surface. The reaction rate and heat generation rate peak at the end of pressurization ramp, after which the reaction becomes localized to colder locations. Thereafter, the reaction rate decreases due to the self-limiting nature of the reaction and high metal hydride temperatures.

The second part of this [13] will discuss the experimental methods used to evaluate the performance of the heat exchanger, and compare the experimental and computational results.

Acknowledgement

This study was partially supported by General Motors Corporation.

References

[1] L. Schlapbach, A. Züttel, Hydrogen-storage materials for mobile applications, Nature 414 (2001) 353–358.
[2] J. Zhang, T.S. Fisher, P.V. Ramachandran, J.P. Gore, I. Mudawar, A review of heat transfer issues in hydrogen storage technologies, J. Heat Transfer 127 (2005) 1391–1399.
[3] G. Walker, Solid-state Hydrogen Storage: Materials and Chemistry, Woodhead Publishing, Cambridge, England, 2008.
[4] M. Visaria, I. Mudawar, T. Pourpoint, S. Kumar, Study of heat transfer and kinetics parameters influencing the design of heat exchangers for hydrogen storage in high-pressure metal hydrides, Int. J. Heat Mass Transfer 53 (2010) 2229–2239.
[5] DOE, Hydrogen, fuel cells and infrastructure technologies program, multi-year research, development and demonstration plan: planned program activities for 2005–2015, Energy Efficiency and Renewable Energy, US Department of Energy, Washington, DC, 2007.
[6] D. Mori, K. Hirose, Recent challenges of hydrogen storage technologies for fuel cell vehicles, Int. J. Hydrogen Energy 34 (2009) 4569–4574.
[7] Y. Kojima, Y. Kawai, S. Towata, T. Matsunaga, T. Shinozawa, M. Kimbara, Development of metal hydride with high dissociation pressure, J. Alloy Compd. 419 (2006) 256–261.
[8] S. Mellouli, F. Askri, H. Dhaou, A. Jemni, S. Ben Nasrallah, A novel design of a heat exchanger for a metal-hydrogen reactor, Int. J. Hydrogen Energy 32 (2007) 3501–3507.
[9] B.D. MacDonald, A.M. Rowe, Impacts of external heat transfer enhancements on metal hydride storage tanks, Int. J. Hydrogen Energy 31 (2006) 1721–1731.
[10] S. Mellouli, F. Askri, H. Dhaou, A. Jemni, S. Ben Nasrallah, Numerical study of heat exchanger effects on charge/discharge times of metal-hydrogen storage vessel, Int. J. Hydrogen Energy 34 (2009) 3005–3017.
[11] A.K. Phate, M.P. Maiya, S.S. Murthy, Simulation of transient heat and mass transfer during hydrogen sorption in cylindrical metal hydride beds, Int. J. Hydrogen Energy 32 (2007) 1969–1981.
[12] F. Laurencelle, J. Goyette, Simulation of heat transfer in a metal hydride reactor with aluminum foam, Int. J. Hydrogen Energy 32 (2007) 2957–2964.
[13] M. Visaria, I. Mudawar, T. Pourpoint, Enhanced heat exchanger design for hydrogen storage using high-pressure metal hydride – Part 2. Experimental results, Int. J. Heat Mass Transfer 54 (2011) 424–432.
[14] U. Mayer, M. Groll, W. Supper, Heat and mass transfer in metal hydride reaction beds: experimental and theoretical results, J. Less-Common Metals 131 (1987) 235–244.
[15] S. Flueckiger, T. Voskuilen, T. Pourpoint, T.S. Fisher, Y. Zheng, In situ characterization of metal hydride thermal transport properties, Int. J. Hydrogen Energy 35 (2010) 614–621.
[16] S. Gustafsson, Transient plane source techniques for thermal conductivity and thermal diffusivity measurements of solid materials, Rev. Sci. Instrum. 62 (1991) 797–804.
[17] S. Suda, Y. Komazaki, N. Kobayashi, Effective thermal conductivity of metal hydride beds, J. Less-Common Metals 89 (1983) 317–324.
[18] S. Suda, N. Kobayashi, K. Yoshida, Reaction kinetics of metal hydrides and their mixtures, J. Less Common Metals 73 (1980) 119–126.